Recovery of Heavy Metal Ions Using Magnetic Glycine-Modified Chitosan–Application to Aqueous Solutions and Tailing Leachate

Asmaa Benettayeb [1,*], Amine Morsli [1,2], Khalid Z. Elwakeel [3,4], Mohammed F. Hamza [5,6] and Eric Guibal [7,*]

[1] Laboratoire de Génie Chimique et de Catalyse Hétérogène, Université de Sciences et de Technologie, Département de Génie Chimique - Mohamed Boudiaf, BP 1505 El-M'Nouer, Oran 31000, Algérie; asma.benettayeb@gmail.com (AB) and (AM)

[2] Laboratoire d'Ingénierie des procédés de l'Environnement (LIPE)- Université des Sciences et Technologie d'Oran - Mohamed Boudiaf", B.P. 1505, El M'Nouer, Oran 31000, Algérie; morsli_amine@yahoo.fr (AM)

[3] University of Jeddah, College of Science, Department of Chemistry, Jeddah 80327, Saudi Arabia; kelwkeel@uj.edu.sa (KZE)

[4] Environmental Science Department, Faculty of Science, Port-Said University, Port Said 42522, Egypt; kelwkeel@uj.edu.sa (KZE)

[5] Guangxi Key Laboratory of Processing for Non-ferrous Metals and Featured Materials, School of Resources, Environment and Materials, Guangxi University, Nanning 530004, China; m_fouda21@hotmail.com (MFH)

[6] Nuclear Materials Authority, POB530, El-Maadi, Cairo, Egypt; m_fouda21@hotmail.com (MFH)

[7] Polymers Composites and Hybrids (PCH), IMT Mines Ales, F-30319 Alès, France; eric.guibal@mines-ales.fr

* Correspondence: eric.guibal@mines-ales.fr (EG) and asma.benettayeb@gmail.com (AB).

Table S1a. Reminder on equations used for modeling uptake kinetics [1-3].

Model	Equation	Parameters	Ref.
PFORE	$q(t) = q_{eq,1}(1 - e^{-k_1 t})$	$q_{eq,2}$ (mmol g^{-1}): sorption capacity at equilibrium k_1 (min^{-1}): apparent rate constant of PFORE	[1]
PSORE	$q(t) = \dfrac{q_{eq,2}^2 k_2 t}{1 + k_2 q_{eq,2} t}$	$q_{eq,2}$ (mmol g^{-1}): sorption capacity at equilibrium k_2 (g mmol^{-1} min^{-1}): apparent rate constant of PSORE	[1]
Elovich	$q(t) = \dfrac{1}{\beta} \ln(1 + \alpha \times \beta \times t)$	α is the initial rate of sorption (mmol g^{-1} min^{-1}) β is the desorption constant (mmol g^{-1})	[3]
RIDE	$\dfrac{q(t)}{q_{eq}} = 1 - \sum_{n=1}^{\infty} \dfrac{6\alpha(\alpha+1)\exp\left(\dfrac{-D_e q_n^2}{r^2}t\right)}{9 + 9\alpha + q_n^2\alpha^2}$ With q_n being the non-zero roots of $\tan q_n = \dfrac{3\,q_n}{3+\alpha q_n^2}$ and $\dfrac{m\,q}{V\,C_0} = \dfrac{1}{1+\alpha}$	D_e (m^2 min^{-1}) : Effective diffusivity coefficient	[2]

(m (g): mass of sorbent; V (L): volume of solution; C_0 (mmol L^{-1}): initial concentration of the solution).

Table S1. b. Reminder on equations used for modeling sorption isotherms [1, 2, 4, 5].

Model	Equation	Parameters	Ref.
Langmuir	$q_{eq} = \dfrac{q_{m,L} C_{eq}}{1 + b_L C_{eq}}$	$q_{m,L}$ (mmol g^{-1}): Sorption capacity at saturation of monolayer b_L (L mmol^{-1}): Affinity coefficient	[1]
Freundlich	$q_{eq} = k_F C_{eq}^{1/n_F}$	k_F and n_F: empirical parameters of Freundlich equation	[4]
Sips	$q_{eq} = \dfrac{q_{m,S} b_S C_{eq}^{1/n_S}}{1 + b_S C_{eq}^{1/n_S}}$	$q_{m,L}$, b_S and n_S: empirical parameters of Sips equation (based on Langmuir and Freundlich equations)	[2]
Temkin	$q_{eq} = \dfrac{RT}{B_T} \ln(A_T C_{eq})$	T (K); R: gas constant; A_T: Temkin binding constant (L mmol^{-1}); B_T: sorption heat (J mol^{-1})	[5]

Akaike Information Criterion, AIC [6]:

$$AIC = N \ln\left(\frac{\sum_{i=0}^{N}(y_{i,exp.} - y_{i,model})^2}{N}\right) + 2N_p + \frac{2N_p(N_p + 1)}{N - N_p - 1}$$

Where N is the number of experimental points, N_p the number of model parameters, $y_{i,exp.}$ and $y_{i,model}$ the experimental and calculated values of the tested variable.

Table S2. Composition of the ore sample collected on the Abu Thor site.

Major Constituents	Wt. %	Trace elements	Content (ppm)
SiO_2	34.15	Cu	9865
Al_2O_3	19.04	U	419
Fe_2O_3	11.43	REE	1098
CaO	7.11	Zn	1394
MgO	4.18	Ni	958
Na_2O	1.99	Co	218
K_2O	1.32	Cd	209
P_2O_5	0.27	V	87
*L.O.I	17.32		

L.O.I.: loss on ignition.

Table S3a. FTIR assignments for glycine.

Wavenumber (cm^{-1})	Assignment	Ref.
3093	NH$_3^+$ str.	[7]
2958	-CH$_3$ asym. str.	[8]
2866	-CH$_3$ sym. str.	[8]
1662 sh.	NH$_3^+$ sym. def. Amide I band (C=O stretching)	[7] [9]
1622 sh.	COO$^-$ asymm. str.	[7]
1574	COO$^-$ asymm. str.	[10]
1494	NH$_3^+$ sym. def. COO-	[7] [11]
1437 w	COO$^-$ sym. str.	[7]
1390	NO$_3$ asymm. str.	[7]
1331	CH$_2$ wag. CH$_2$ in-plan bend.	[10, 11]
1126	N-N rock. NH$_3^+$ rock	[7]
1034	C-N str.	[11]
926	CH$_2$ rock. C-H bend. CH$_2$ out-of-plan bend	[7, 11] [10]
889	C-C str.	[7]
685	COO$^-$	[7]
606	C-H bend.	[12]
499	COO$^-$ def.	[7]

Table S3b. FTIR assignments for chitosan.

Wavenumber (cm^{-1})	Assignment	Ref.
3317-3271	N-H str., O-H str. (overlapped)	[13]
2889	C-H sym. str.	[14]
2868	C-H asym. str.	[14]
1648	C=O str. (Amide I)	[14]
1578	N-H bend. (Amide II), N-H bend. (primary amine)	[14]
1423	CH$_2$ bend.	[14]
1383	CH$_3$ sym. def., -C-O str. (primary alcoholic group)	[14, 15]
1149	C-O-C bridge asym. str.	[14]
1061	C-O str., primary OH groups, carbohydrate ring	[14]
893	C-H out-of-plane bend.	[16]
658	-NH twist	[16]

Table S3c. FTIR assignments for MCh.

Wavenumber (cm^{-1})	Assignment	Ref.
2913	C-H sym. str. (CH_2)	[17]
2856	C-H asym. str.	[14]
1558	NH_2 def., NH_2 sci. (primary amine)	[18]
1398	C-H asym. bend.	[18]
1147	C-O-C bridge asym. str.	[14]
1063	C-O str., primary OH groups	[14, 17]
1012	Carbohydrate ring	[14]
891	C-H out-of-plane bend.	[16]
546-559	Fe-O-Fe str.	[15, 19]

Table S3d. FTIR assignments for MChs and MChs*.

Wavenumber (cm^{-1})		Assignment	Ref.
MCh	MChs		
2912/2923	2918	C-H sym. str. (CH_2)	[17]
2868	2868	C-H asym. str.	[14]
1624	1653	-NH bending (secondary amine)	[8]
1524	-	NH_2 def./sci.	[18]
1375	1375	C-H asym. bend.	[18]
1149	1149	C-O-C bridge asym. str.	[14]
1055	1060	C-O str., primary OH groups	[14, 17]
1032	1032	Carbohydrate ring	[14]
897	897	C-H out-of-plane bend.	[16]
561	561	Fe-O-Fe str.	[15, 19]

Table S3e. FTIR assignments for G@MChs.

Wavenumber (cm^{-1})	Assignment	Ref.
2926	C-H sym. str. (CH_2)	[17]
2875	C-H asym. str.	[14]
1635/1626	-NH bending (secondary amine) COO$^-$ asymm. str.	[8] [7]
1541	NH_2 def./sci.	[18]
1456	CH_2 bend.	[14]
1375	C-H asym. bend.	[18]
1319	=C-H bend.	[8]
1149	C-O-C bridge asym. str.	[14]
1057	C-O str., primary OH groups	[14, 17]
1033	Carbohydrate ring	[14]
986 w,sh	Carbohydrate ring	[14]
897	C-H out-of-plane bend.	[16]
798	Shifted C-C from Glycine and methylene rocking	[8]
563	Fe-O-Fe str.	[15, 19]

**Table S4.** Physico-chemical properties of selected metals [20, 21].

Metal	χ_{aq}	R_p (Shannon, Å)	$-\Delta G°_{hydr.}$ (kcal mol^{-1})	Softness	pK_s	Pearson' ranking	Aqua Complex (a)
Ni(II)	2.891	0.69	473.2	-0.11	14.7	B	6 o
Cu(II)	2.952	0.73	480.4	0.38	19.3	B	6 o
Hg(II)	2.958	1.02	420.7	1.27	25.4	S	6 o
Zn(II)	2.796	0.75	467.3	0.35	17.0	B	6 o
Cd(II)	2.660	0.95	419.5	0.58	13.7	S	6 o
Pb(II)	2.478	1.19	340.6	0.41	15.1	B	6 v
U(VI)	-	1.08	-	-0.27	-	H	5 dpbp
Fe(III)	3.835	0.65	1019.4	0.33	38.6	H	6 o
Al(III)	3.435	0.53	1081.5	-0.31	31.0	H	6 o
Nd(III)	3.085	1.16	783.9	-0.58	25.2	H	9 ttp
Sm(III)	3.232	1.13	794.7	-0.36	-	H	9 ttp
Y(III)	2.829	1.02	824.6	-0.69	23.3	H	8 sa

Aqua complex: Me(H$_2$O)$_a^{i+}$; t: tetrahedron, o: octahedron, v: variable, sa: square antiprism, ttp: tricapped trigonal prism, dpbp: distorted pentagonal bipyramid.
Carboxyl (O): H - Amine (N): B – S-based: S

Table S5. Composition of ore leachates (before and after pre-treatments; concentrations, mg L^{-1}).

Element	Concentration	Concentration after pH control to 4	Concentration after sorption step*
Cd	57.08	42.29	4.0
Zn	509.64	492	477
Cu	1126.9	1078.4	927
Ni	301.5	266.2	80.6
U	105.48	96.4	60.0
Al	10219	3370	2802
Fe	8731	184.3	79.3
Pb			
Co	66.65	54.3	4.0
TREE	163.4	157.4	38.1
Nd			16.0
Sm			5.8
Y			4.0

*: sorption step using DOWEX 50X8 cationic commercial resin at pH 4.
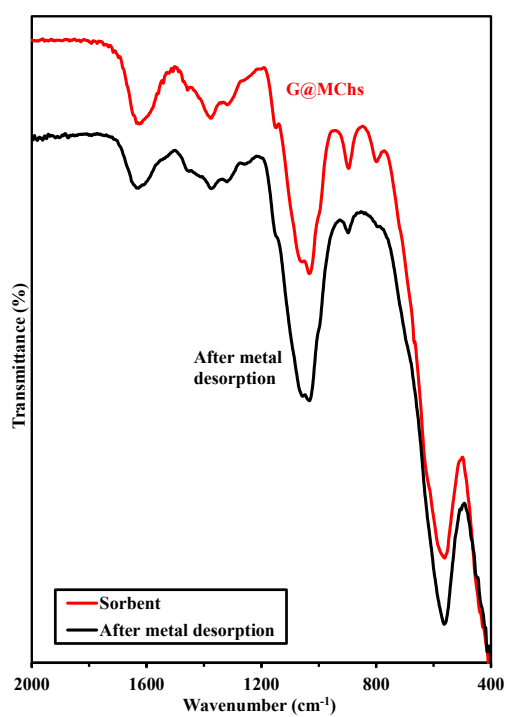
Figure S1. Comparison of FTIR spectrum of pristine G@MChs with the spectrum of the sorbent after metal desorption.
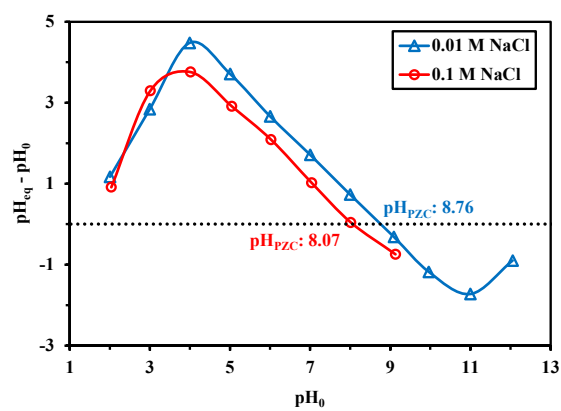
Figure S2. Determination of pH_{PZC} (pH-drift method, NaCl as background salt at 2 concentrations: 0.1 and 0.01 M; Sorbent dose, SD: 1 g L^{-1}; v: 150 rpm; T: 21 ±1 °C, time: 48 h).
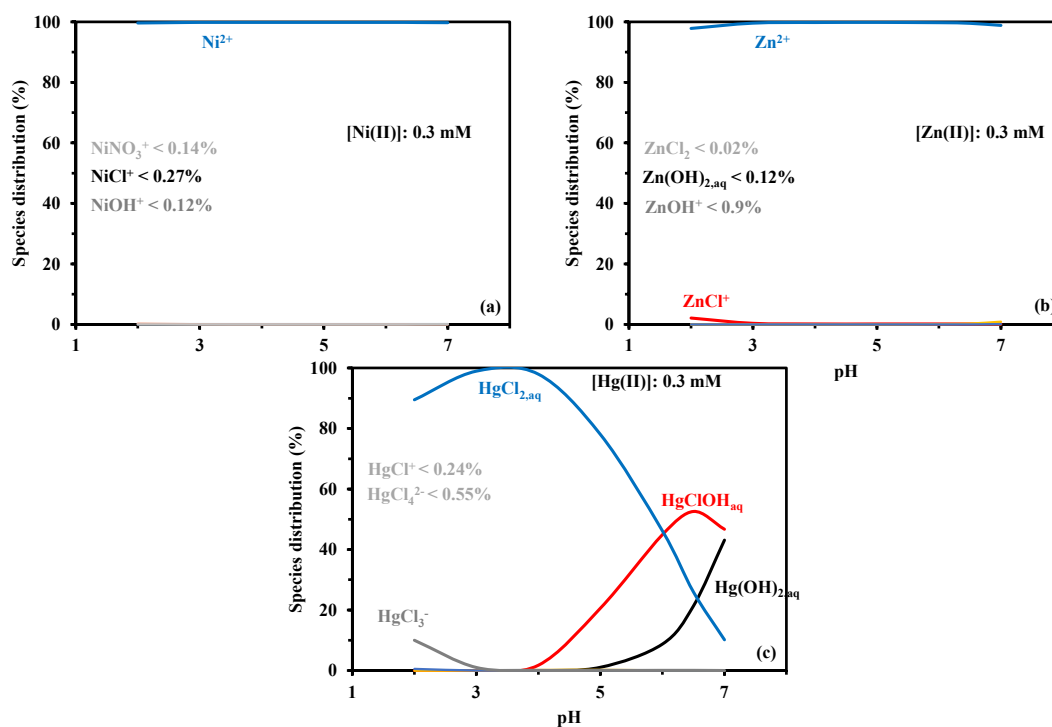
Figure S3. Speciation diagrams for Ni(II), Zn(II), and Hg(II) under the experimental conditions selected for the study of pH effect (calculations with Visual Minteq, [22]).
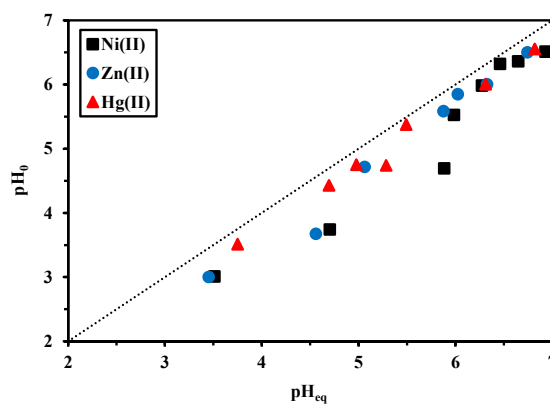
Figure S4. pH variation during the sorption of Ni(II), Zn(II), and Hg(II) using G@MChs (C_0: 0.3 mmol L^{-1}; Sorbent dose, SD: 1 g L^{-1}; T: °C; time: 480 min; agitation speed: 150 rpm).
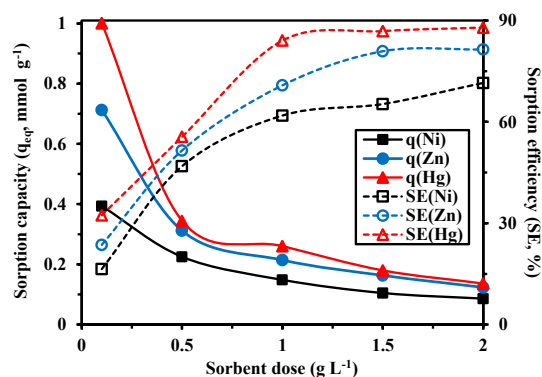
Figure S5. Effect of sorbent dose on the sorption of Ni(II), Zn(II) and Hg(II) using G@MChs (C_0: 0.3 mmol L^{-1}; pH_0: ~5.5; pH_{eq}: ~5.8-6.3; T: 21 ±1 °C; time: 480 min; agitation speed: 150 rpm).
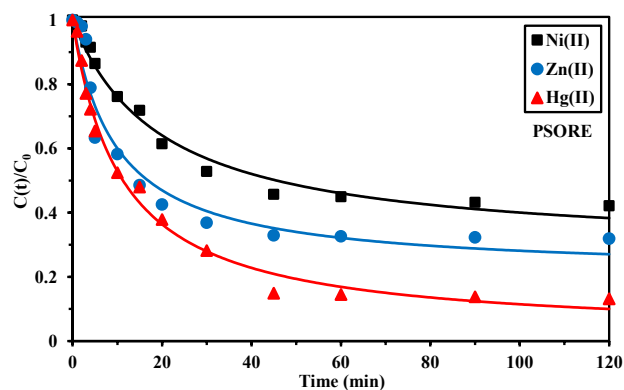
Figure S6. Uptake kinetics for Ni(II), Zn(II) and Hg(II) using G@MChs – Modeling with the PSORE (C_0: 0.3 mmol L^{-1}; pH_0: 5.5; pH_{eq}: 5.75 (Ni), 5.80 (Zn), and 6.01 (Hg); Sorbent dose, SD: 1 g L^{-1}; T: °C; time: h; agitation speed: 150 rpm).
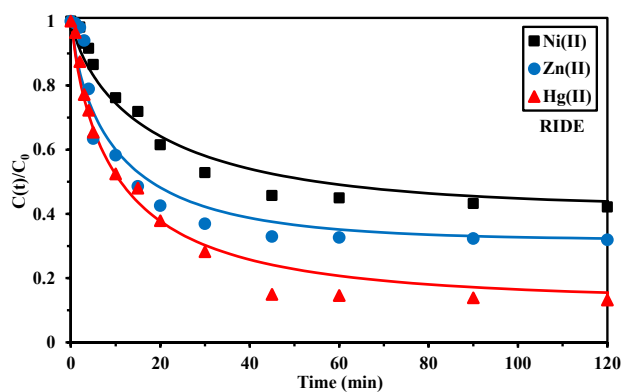
Figure S7. Uptake kinetics for Ni(II), Zn(II) and Hg(II) using G@MChs – Modeling with the RIDE (C_0: 0.3 mmol L^{-1}; pH_0: 5.5; pH_{eq}: 5.75 (Ni), 5.80 (Zn), and 6.01 (Hg); Sorbent dose, SD: 1 g L^{-1}; T: 21 ±1 °C; time: 300 min; agitation speed: 150 rpm).
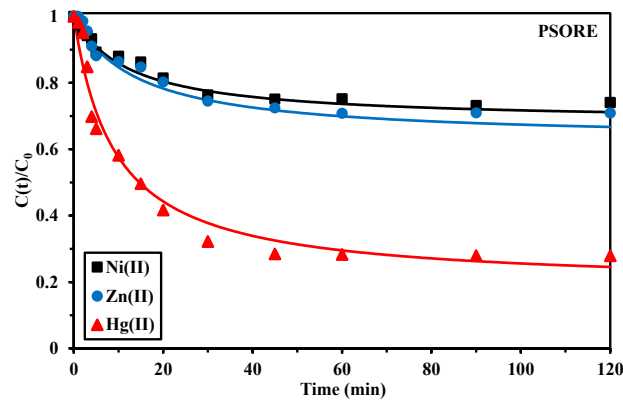
Figure S8. Uptake kinetics for Ni(II), Zn(II) and Hg(II) using G@MChs from multi-component solutions – Modeling with the PSORE (C_0: 0.3 mmol L^{-1}; pH_0: 5.5; pH_{eq}: 5.75 (Ni), 5.80 (Zn), and 6.01 (Hg); Sorbent dose, SD: 1 g L^{-1}; T: 21 ±1 °C; time: 300 min; agitation speed: 150 rpm).
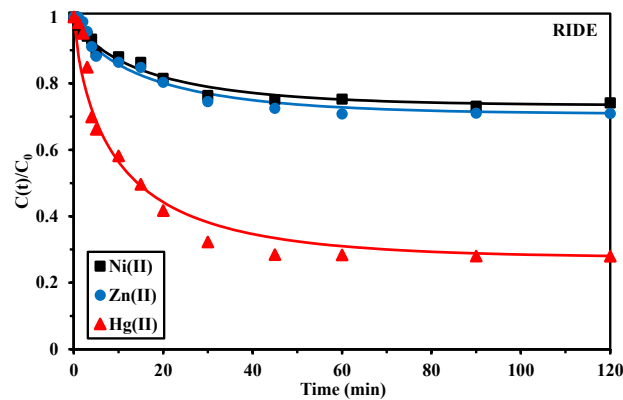
Figure S9. Uptake kinetics for Ni(II), Zn(II) and Hg(II) using G@MChs from multi-component solutions – Modeling with the RIDE (C_0: 0.3 mmol L^{-1}; pH_0: 5.5; pH_{eq}: 5.75 (Ni), 5.80 (Zn), and 6.01 (Hg); Sorbent dose, SD: 1 g L^{-1}; T: 21 ±1 °C; time: 300 min; agitation speed: 150 rpm).
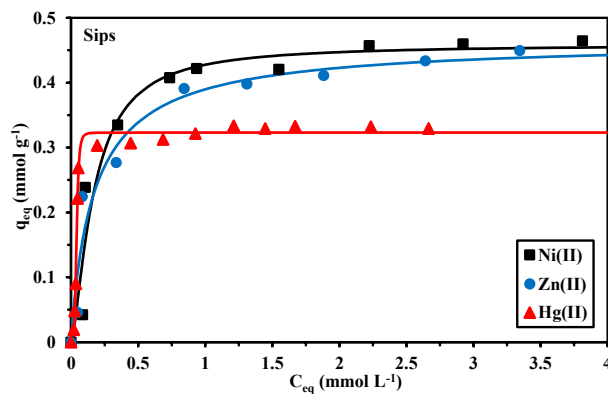
Figure S10. Sorption isotherms for Ni(II), Zn(II) and Hg(II) using G@MChs for single-component solutions – Modeling with the Sips equation (C_0: 0.3 mmol L^{-1}; pH_0: 5.5; pH_{eq}: 5.75 (Ni), 5.80 (Zn), and 6.01 (Hg); Sorbent dose, SD: 1 g L^{-1}; T: 21 ±1 °C; time: 60 min; agitation speed: 150 rpm).
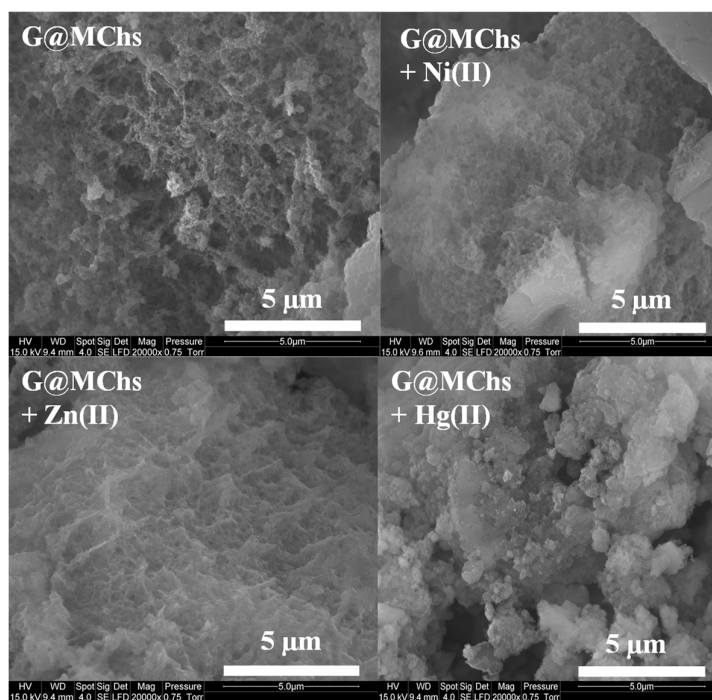
Figure S11. SEM micrographs of sorbent before and after sorption of Ni(II), Zn(II) and Hg(II).
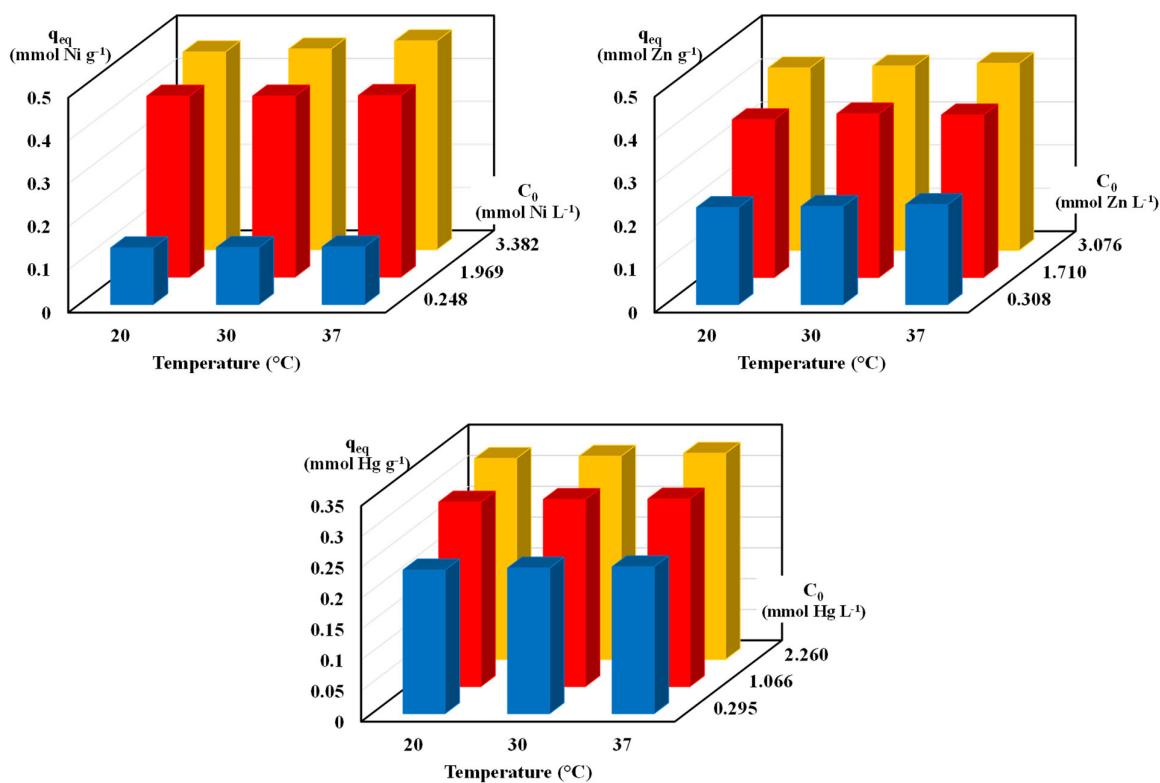
Figure S12. Effect of temperature on the sorption of Ni(II), Zn(II) and Hg(II) using G@MChs at different initial metal concentrations (C₀; pH₀: 5.5; SD: 1 g L⁻¹; v: 150 rpm; time: 480 min).
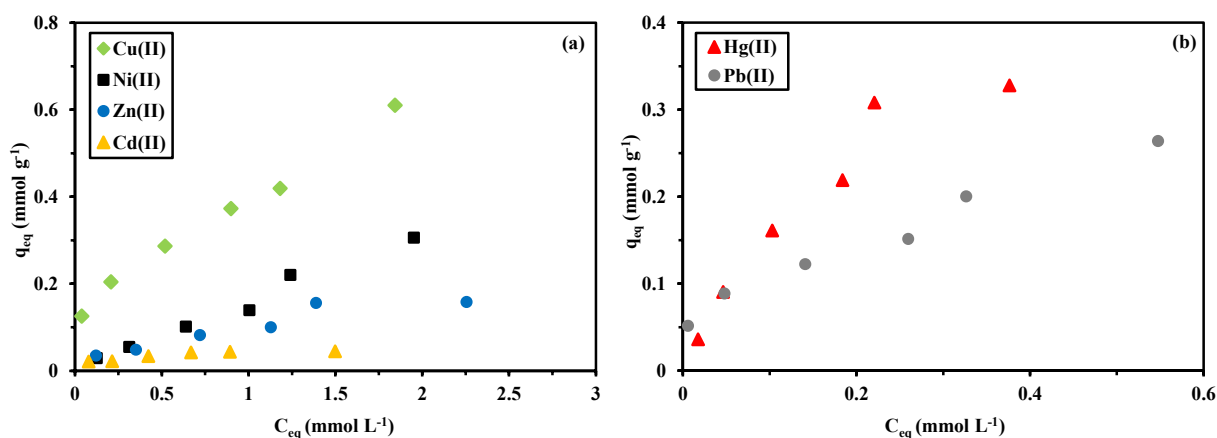
Figure S13. Metal sorption onto G@MChs from multi-component solutions (pH$_0$: 5.5; SD; 1 g L^{-1}; C$_0$: 10-156 mg Cu L^{-1}, 10-142 mg Hg L^{-1}, 9-133 mg Ni L^{-1}, 12-168 mg Pb L^{-1}, 11-173 mg Cd L^{-1}, 10-158 mg Zn L^{-1}; T: 21 ±1 °C; time: 480 min).
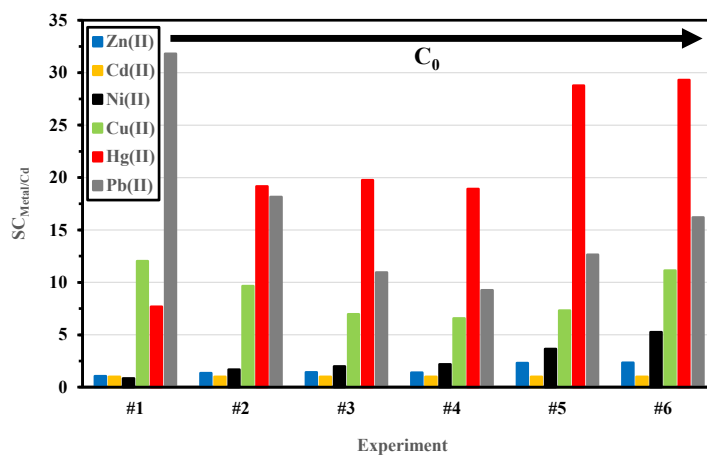
Figure S14. Selectivity coefficient (SC$_{Metal/Cadmium}$) (effect of increasing initial concentration) (experimental conditions, see Figure S13).
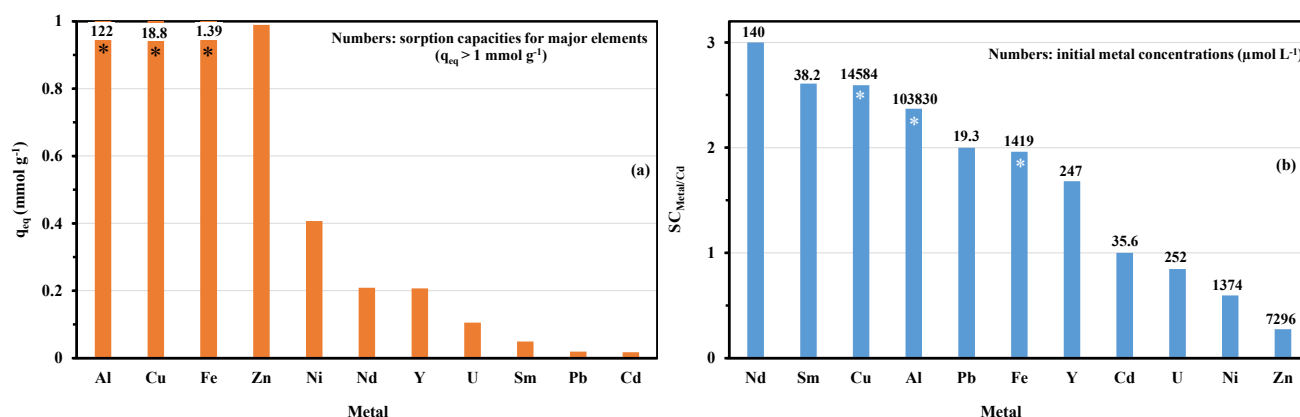
Figure S15. Treatment of ore leachate – (a) sorption capacities and (b) selectivity coefficients (pH$_0$ 5.5, SD: 0.5 g L^{-1}; time: 24 h; agitation speed: 150 rpm; T: 21 ±1 °C; star *: probable occurrence of metal precipitation).

References

1. Ho, Y. S.; McKay, G., Pseudo-second order model for sorption processes. *Process Biochem.* **1999,** 34, (5), 451-465.
2. Tien, C., *Adsorption Calculations and Modeling*. Butterworth-Heinemann: Newton, MA, 1994 p243.
3. Zhang, R.; Leiviska, T., Surface modification of pine bark with quaternary ammonium groups and its use for vanadium removal. *Chem. Eng. J.* **2020,** 385, Art. N° 123967.
4. Freundlich, H. M. F., Uber die adsorption in lasungen. *Z. Phys. Chem.* **1906,** 57, 385-470.
5. Temkin, M. I.; Pyzhev, V., Kinetics of ammonia synthesis on promoted iron catalysts. *Acta Physiochim.* **1940,** 12, (1), 217-222.
6. Falyouna, O.; Eljamal, O.; Maamoun, I.; Tahara, A.; Sugihara, Y., Magnetic zeolite synthesis for efficient removal of cesium in a lab-scale continuous treatment system. *J. Colloid Interface Sci.* **2020,** 571, 66-79.
7. Hernandez-Paredes, J.; Glossman-Mitnik, D.; Esparza-Ponce, H. E.; Alvarez-Ramos, M. E.; Duarte-Moller, A., Band structure, optical properties and infrared spectrum of glycine-sodium nitrate crystal. *J. Mol. Struct.* **2008,** 875, (1-3), 295-301.
8. Coates, J., Interpretation of Infrared Spectra, A Practical Approach. In *Encyclopedia of Analytical Chemistry* John Wiley & Sons, Ltd.: 2006; pp 1-23.
9. Balan, V.; Mihai, C. T.; Cojocaru, F. D.; Uritu, C. M.; Dodi, G.; Botezat, D.; Gardikiotis, I., Vibrational spectroscopy fingerprinting in medicine: from molecular to clinical practice. *Materials* **2019,** 12, (18), Art. N° 12182884.
10. Olsztynska-Janus, S.; Gasior-Glogowska, M.; Szymborska-Malek, K.; Czarnik-Matusewicz, B.; Komorowska, M., Specific applications of vibrational spectroscopy in biomedical engineering. In *Biomedical Engineering, Trends, Research and Technologies*, Komorowska, M. A.; OlsztynskaJanus, S., Eds. Intechopen: London (UK), 2011; pp pp. 91-120.
11. Latha, A. A.; Anbuchezhiyan, M.; Kanakam, C. C.; Selvarani, K., Synthesis and characterization of γ-glycine - a nonlinear optical single crystal for optoelectronic and photonic applications. *Mater. Sci. - Poland* **2017,** 35, (1), 140-150.
12. Venkatesan, G.; Pari, S., Growth of glycine ethyl ester hydrochloride and its characterizations. *Physica B* **2016,** 501, 26-33.
13. Wang, X.; Tang, R.; Zhang, Y.; Yu, Z.; Qi, C., Preparation of a novel chitosan based biopolymer dye and application in wood dyeing. *Polymers* **2016,** 8, (9), Art. N° 8090338.
14. Queiroz, M. F.; Teodosio Melo, K. R.; Sabry, D. A.; Sassaki, G. L.; Oliveira Rocha, H. A., Does the use of chitosan contribute to oxalate kidney stone formation? *Mar. Drugs* **2015,** 13, (1), 141-158.
15. Zhou, Z.; Jiang, F.; Lee, T.-C.; Yue, T., Two-step preparation of nano-scaled magnetic chitosan particles using Triton X-100 reversed-phase water-in-oil microemulsion system. *J. Alloys Compd.* **2013,** 581, 843-848.
16. Song, C.; Yu, H.; Zhang, M.; Yang, Y.; Zhang, G., Physicochemical properties and antioxidant activity of chitosan from the blowfly Chrysomya megacephala larvae. *Int. J. Biol. Macromol.* **2013,** 60, 347-354.
17. Sahbaz, D. A.; Yakar, A.; Gunduz, U., Magnetic Fe$_3$O$_4$-chitosan micro- and nanoparticles for wastewater treatment. *Part. Sci. Technol.* **2019,** 37, (6), 728-736.
18. Pylypchuk, I. V.; Kolodynska, D.; Gorbyk, P. P., Gd(III) adsorption on the DTPA-functionalized chitosan/magnetite nanocomposites. *Sep. Sci. Technol.* **2018,** 53, (7), 1006-1016.
19. Stoia, M.; Istratie, R.; Păcurariu, C., Investigation of magnetite nanoparticles stability in air by thermal analysis and FTIR spectroscopy. *J. Therm. Anal. Calorim.* **2016,** 125, (3), 1185-1198.
20. Persson, I., Hydrated metal ions in aqueous solution: How regular are their structures? *Pure Appl. Chem.* **2010,** 82, (10), 1901-1917.
21. Li, K.; Li, M.; Xue, D., Solution-phase electronegativity scale: Insight into the chemical behaviors of metal ions in solution. *J. Phys. Chem. A* **2012,** 116, (16), 4192-4198.
22. Gustafsson, J. P. *Visual MINTEQ*, ver. 3.1; KTH, Royal Institute of Technology: Stockholm, Sweden, 2013.